5. Double Layers in Astrophysics

Double layers were discovered by Irving Langmuir (who called them "double sheathes") in his experiments with low-pressure discharges in the 1920s. Subsequently, they were observed by nearly all the pioneers in experimental plasma physics [Tonks 1937, Schönhuber 1958, Crawford and Freeston 1963, Babi´c et al. 1971]. The double layer consists of two thin and close regions of opposite charge excess which give rise to a potential drop, and therefore an electric field, across the layer. H. Alfvén first advocated the existence of double layers in cosmic settings (1958), but proof of their existence in the earth's magnetosphere did not come until potential probes on earth satellites made in situ measurements two decades later.

5.1 General Description of Double Layers

The basic phenomena under study in this chapter is illustrated in Figure 5.1. Electrons and ions counterflow with velocities v_{e0} and v_{i0}, respectively, or with a relative drift velocity $V_0 = v_{e0} + v_{i0}$. Because of this counterflow, an instability or instabilities are set up within the current. The net result is a reconfiguration of the current carrying charges over a narrow region so as to cause a potential drop. Because of the potential drop a beam of electrons with instantaneous velocity v_{eb} is accelerated to the right while a beam of ions with instantaneous velocity v_{ib} is accelerated to the left. The phenomenon responsible for this behavior is called a *double layer*.

The classic double layer (DL) [Langmuir 1929] is therefore an electrostatic structure which can appear within a current carrying plasma and sustain a significant net potential difference. The thickness is of the Debye length scale and can be very small compared to the dimensions of the region in which the DL is embedded. Internally the DL is not charge neutral and must contain at least two layers of opposite net charge (hence the term "double layer") associated with an internal electric field.

Four populations of particles are required to produce the space-charge distribution needed to support the double layer potential. These are (i) the current-carrying streaming electrons, (ii) the current-carrying streaming ions, (iii) trapped electrons on the downstream side of the streaming electrons, and (iv) trapped ions on the downstream side of the streaming ions.

Figure 5.2 is a sketch of the potential profile, the four-particle populations, and their contributions to the space-charge distribution to support the double layer potential. The streaming electrons and ions are present because the field-aligned current is an essential ingredient of a double layer. Due to the acceleration of the streaming particles by the double layer potential, the density of each streaming particle population decreases on the downstream side. Therefore, trapped particles must be produced to ensure overall charge neutrality.

Because electrical currents in astrophysical settings are often aligned along magnetic fields,

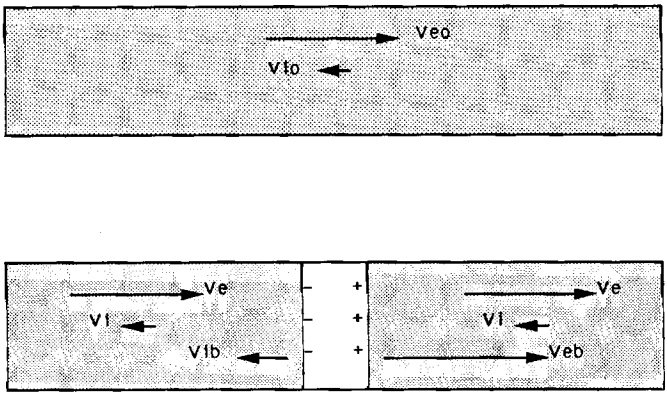

Figure 5.1. **(top)** Condition for the development of a double layer. **(bottom)** A double layer.

the internal electric field has a component parallel to the magnetic field. Thus, the DL is a region where ideal magnetohydrodynamics breaks down. As a whole the DL has no net charge and the surrounding plasma may be perturbed by extended presheaths matching the conditions at the edges of the DL to those in the undisturbed plasma.

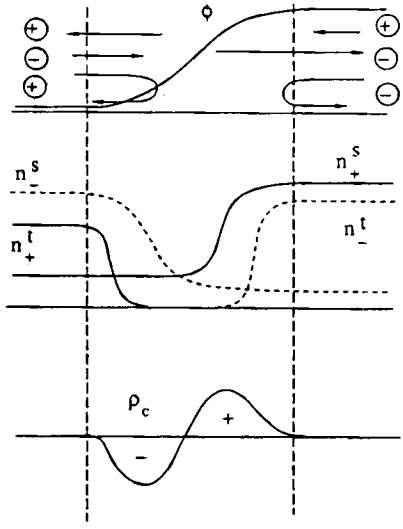

Figure 5.2. A sketch of the double layer potential ϕ, the trapped and streaming ions and electrons, the space charge due to each of the four populations of particles, and the net space charge required to support the double layer potential.

A basic property, which is of particular interest for applications to astrophysics, is that particles traversing the DL are directly accelerated by the net potential difference, ϕ_{DL}. The DL acts as an electrical load dissipating energy at a rate $I\,\phi_{DL}$ (where I is the total current through the DL), which is transformed to the directed kinetic energy of accelerated particles. Thus, the DL exhibits inertial resistance. This should be contrasted with the effect of ohmic or anomalous resistance, which is to transform electrical energy to thermal or random particle motions. Since the DL acts as a load, there has to be an external source maintaining the potential difference ϕ_{DL} and driving the current I. In the laboratory this source is usually an electrical power supply, whereas in space it may be the magnetic energy stored in an extended current system Eq.(3.36), which responds to a change in current with an inductive voltage.

The material in this chapter is based primarily on the in-depth reviews of Block (1978), Carlqvist (1982, 1986), Borovsky (1984), and Raadu (1989).

5.2 The Time-Independent Double Layer

5.2.1 One-Dimensional Model

It is instructional to first consider a one-dimensional, time-independent model of a double layer with a high potential drop [Carlqvist 1986]. In this model the layer is situated between the cathode boundary at $x = 0$ and the anode boundary at $x = d$ (Figure 5.3). The potential is set $\phi = 0$ at $x = 0$ and $\phi = \phi_{DL}$ at $x = d$ so that the potential drop across the layer is ϕ_{DL}. Electrons and ions are emitted with zero velocity from the cathode boundary and anode boundary, respectively.

The ions and electrons inside the double layer are accelerated in opposite directions along the magnetic field by the electric field. The ions accelerate towards the cathode while the electrons accelerate towards the anode. Since the initial velocity of the particles is zero, conservation of energy dictates the potential energy be balanced by the kinetic energy so that

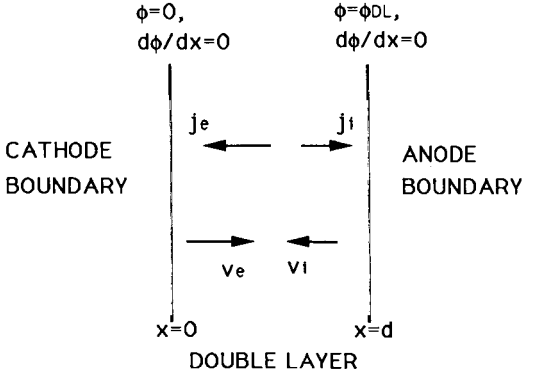

Figure 5.3. Schematic of a one-dimensional double layer model. The DL has the thickness d and sustains a potential drop ϕ_{DL}. Ions and electrons are emitted with zero velocity from the anode boundary and cathode boundary, respectively, and accelerated in opposite directions by a strong electric field.

$$Ze\phi' = m_i c^2(\gamma_i - 1) \tag{5.1}$$

for the ions, and

$$e\phi = m_e c^2 (\gamma_e - 1) \tag{5.2}$$

for the electrons, where Ze is the ion charge and the Lorentz factors are $\gamma_i = (1-\beta_i^2)^{-1/2}$, and $\gamma_e = (1-\beta_e^2)^{-1/2}$ for ion and electron velocities β_i and β_e [Eq.(8.18)], respectively.

At the potentials ϕ and ϕ, β_i and β_e are given by

$$\beta_i = \frac{\left(\phi'^2 + 2\phi_i \phi\right)^{1/2}}{\phi_i + \phi'} \tag{5.3}$$

and

$$\beta_e = \frac{-\left(\phi^2 + 2\phi_e \phi\right)^{1/2}}{\phi_e + \phi} \tag{5.4}$$

where $\phi_e = m_e c^2/e = 511$ kV is the rest mass energy of electrons, $\phi_i = m_i c^2/Ze = 0.939$ GV is the rest mass energy of ions, and $\phi = \phi_{DL} - \phi$.

The current densities of the ions and electrons are

$$j_i = Zen_i \beta_i c$$

and

$$j_e = -en_e \beta_e c$$

respectively. Combining Eqs.(5.1) and (5.2) with Eqs.(5.3) and (5.4) and inserting the particle densities in Poisson's equation, we find

$$\frac{d^2\phi}{dx^2} = -\frac{e(Zn_i - n_e)}{\varepsilon_0}$$

$$= \frac{j_e}{\varepsilon_0 c} \frac{\phi_e + \phi}{\left(\phi^2 + 2\phi_e\phi\right)^{1/2}} - \frac{j_i}{\varepsilon_0 c} \frac{\phi_i + \phi'}{\left(\phi'^2 + 2\phi_i\phi\right)^{1/2}} \tag{5.5}$$

Multiplying both sides of Eq.(5.5) with $2d\phi/dx = -2d\phi'/dx$ and integrating, yields,

$$\left(\frac{d\phi}{dx}\right)^2 = \frac{2j_e}{\varepsilon_0 c}\left(\phi^2 + 2\phi_e\phi\right)^{1/2} + \frac{2j_i}{\varepsilon_0 c}\left(\phi'^2 + 2\phi_i\phi\right)^{1/2} - C_1 \tag{5.6}$$

This equation describes the momentum balance in the layer and may be cast in a more familiar form

$$n_i \gamma_i m_i v_i^2 + n_e \gamma_e m_e v_e^2 - \frac{1}{2}\varepsilon_0 E^2 = C_1$$

The constant of integration C_1 is obtained by inserting the boundary conditions $d\phi/dx = 0$ for $\phi = 0$ and $\phi = \phi_{DL}$ in Eq.(5.4). This is given by

$$C_1 = \frac{2j_e}{\varepsilon_0 c}\left(\phi_{DL}^2 + 2\phi_e\phi_{DL}\right)^{1/2} = \frac{2j_i}{\varepsilon_0 c}\left(\phi_{DL}^2 + 2\phi_i\phi_{DL}\right)^{1/2} \tag{5.7}$$

5.2.2 Ratio of the Current Densities

From Eq.(5.7) the ratio of the ion current density to the electron current density is

$$\boxed{\frac{j_i}{j_e} = \left(\frac{\phi_{DL} + 2\phi_e}{\phi_{DL} + 2\phi_i}\right)^{1/2}} \tag{5.8}$$

For the nonrelativistic double layer $\phi_{DL} << \phi_e \lesssim \phi_i$ and Eq.(5.8) reduces to [Carlqvist 1982]

$$\frac{j_i}{j_e} \approx Z^{1/2}\left(\frac{m_e}{m_i}\right)^{1/2} \tag{5.9}$$

Equation (5.9) is referred to as the *Langmuir condition*. For relativistic double layers $(\phi_{DL} >> \phi_i \gtrsim \phi_e)$, and Eq.(5.8) reduces to

$$\frac{j_i}{j_e} \approx 1 - \frac{\phi_i}{\phi_{DL}} + \frac{\phi_e}{\phi_{DL}} \approx 1 \tag{5.10}$$

5.2.3 The Potential Drop

We can integrate Eq.(5.6) to find the potential drop of the double layer as a function of the total current density $j = j_i + j_e$ and the thickness of the layer d. For nonrelativistic double layers, Langmuir (1929) found by numerical integration

$$\phi_{DL} = \left\{ \frac{9}{4\varepsilon_0 C_2} \left(\frac{m_e}{2e}\right)^{1/2} \left[1 + \left(Z\frac{m_e}{m_i}\right)\right]^{-1} j d^2 \right\}^{2/3} \tag{5.11}$$

Here C_2 is a constant having the value 1.865 [Raadu 1982].

For relativistic double layers a direct integration of Eq.(5.6) yields

$$\phi_{DL} = \left(\frac{\phi}{4\varepsilon_0 c} j d^2 \right)^{1/2} \tag{5.12}$$

The potential drop of both the nonrelativistic and relativistic double layers depend on the product jd^2. Note also that the relativistic double layer is strongly influenced by the mass-to-charge ratio of the ions. In Figure 5.4 the double layer potential ϕ_{DL} has been plotted as a function of jd^2 for double layers carrying electrons and two kinds of ions (H^+, Fe^+). Included in the figure is also a layer which, instead of ions, carries positively charged dust grains (Appendix C). The mass and charge chosen for the grains are $m_g = 10^{-20}$ kg and $Z_g e = 10^2 e$, respectively, being constant with a radius $r_g = 1.4 \times 10^{-8}$ m, a density of $\rho_{mg} = 10^3$ kg m^{-3}, and a potential $\phi_g = 10$ V of the grains.

5.2.4 Structure of the Double Layer

The charge distributions in the relativistic double layer are illustrated in Figure 5.5. The density of the positive charges Zn_i shows a spike close to the anode surface and is almost constant in the rest of the double layer. The spike is caused by rapid ion acceleration away from the anode. A similar variation is found for the electron density n_e near the cathode surface. The negative spike is much thinner than the positive spike because of the smaller mass of the electrons. In order for charge neutrality to prevail in the layer as a whole, the almost constant charge level of the electrons must be slightly larger than that of the ions. The charge distribution in the layer consists, approximately, of a positive surface charge at the anode surface and a small and uniform negative charge density in the rest of the layer. For a constant current density, the density of the surface charge remains constant and independent of the thickness of the relativistic layer.

5.2.5 Kinetic Description

Mathematically, double layers are a subset of the Bernstein–Greene–Kruskal (BGK) solutions [Ichimaru 1973] of the Poisson–Vlasov equations for constant-profile electrostatic potential structures, moving at a constant speed or stationary in a plasma. The BGK solutions include double layers, electrostatic shocks, ion-acoustic solitons, and nonlinear wave trains of any potential form. In the moving frame of a constant-profile constant-speed potential structure, the Vlasov equation [Eq.(2.1) in the absence of collisions] becomes time independent and can be written as

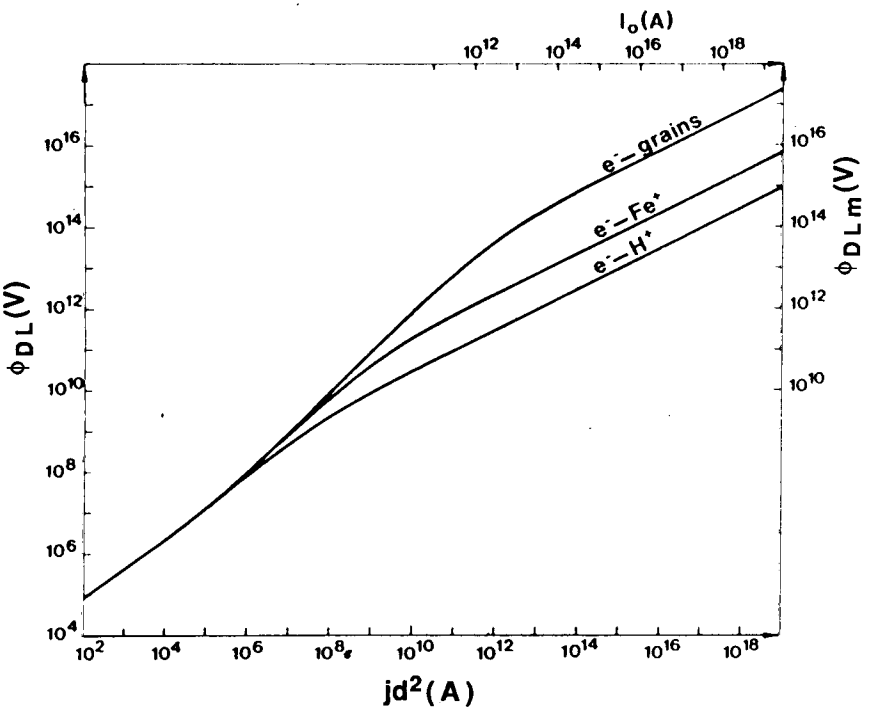

Figure 5.4. Potential drop ϕ_{DL} (left-hand vertical scale) as a function of jd^2 (lower horizontal scale) shown for three strong one-dimensional double layers consisting of (1) electrons and protons, (2) electrons and singly ionized iron ions, and (3) electrons and dust grains of mass $m_g = 10^{-2}$ kg and positive charge 10^2 e. Notice that the three curves practically coincide in the nonrelativistic regime but differ significantly in the relativistic regime. The diagram also illustrates the maximum potential drop ϕ_{DLm} (right-hand vertical scale) as a function of the filamentary current I_0 (upper horizontal scale) for relativistic double layers in a current filament (courtesy of P. Carlqvist).

$$v\frac{\partial f_s}{\partial x} - \frac{q_s}{m_s}\frac{\partial \phi}{\partial x}\frac{\partial f_s}{\partial v} = 0 \tag{5.13}$$

where the subscript denotes the particle species f_s is the distribution function, and ϕ is the electrostatic potential. Solutions of the time-independent Vlasov equation, f_s can be any function of the constants of particle motion. In an unmagnetized plasma, a constant of the motion is the total energy (i.e., the sum of the kinetic and potential energies). Hence a general solution of Eq.(5.13) can be written as

$$f_s = f_s\left(v^2 + 2q_s\,\phi / m_s\right) \tag{5.14}$$

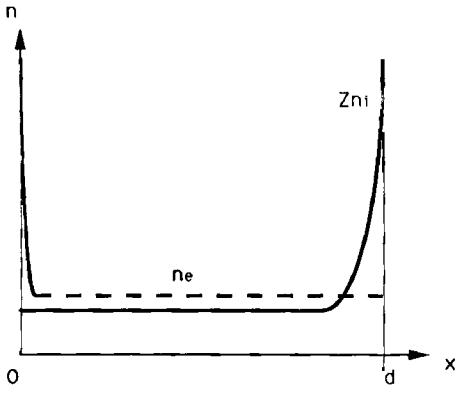

Figure 5.5. Schematic diagram illustrating the densities of positive ion charges Zn_i, and of negative charges (electrons) n_e as a function of x for a one-dimensional DL. The resulting charge distribution may roughly be described as a positive surface charge at the anode boundary $x = d$, and an equal but negative charge distributed uniformly in the rest of the DL.

The number densities of the electrons and ions can be calculated from the distribution function f_s. Thus, using Eq.(2.2) in velocity space, Poisson's equation Eq.(1.3) can be written as [Kan and Akasofu 1989]

$$\frac{\partial^2 \phi}{\partial x^2} = \frac{e}{\varepsilon_0}\left[\int_{-\infty}^{\infty} d^3\mathrm{v}\, f_e - \int_{-\infty}^{\infty} d^3\mathrm{v}\, f_i\right]$$

$$= \frac{e}{\varepsilon_0}\left[n_e(\phi) - n_i(\phi)\right]$$

$$= \Psi(\phi) \qquad (5.15)$$

where the number densities n_e and n_i are functions of the electrostatic potential ϕ, as can be seen from Eq.(5.14) upon integration over the velocity space. The third equality is just a further simplification in notation. A standard method for solving the nonlinear differential of the type of Eq.(5.15) is to treat it as an equation of motion for the fictitious particle in a pseudo potential Ψ, in which "ϕ" is taken to be the "coordinate" and "x" is taken to be the "time." The double layer solution to Eq.(5.15) exists if $\Psi(\phi)$ has the appropriate form as shown in Figure 5.6. In this case, the fictitious particle which starts from point A will roll down the potential well Ψ and climb back up to stay at point B. As the fictitious particle moves from A to B in Figure 5.6, the electrostatic potential ϕ makes a monotonic transition from ϕ_A to ϕ_B as required by the double layer. To ensure that ϕ_A and ϕ_B are asymptotic states of the double layer potential, Ψ must be maxima at points A

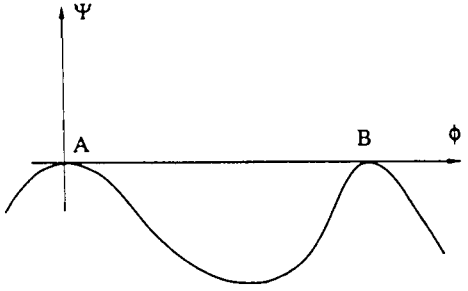

Figure 5.6. A sketch of the pseudo potential Ψ as a function of the double layer potential ϕ.

and B. To ensure that the transition from A to B can take place, Ψ must have a minimum between A and B. Thus, the conditions for the existence of double layer solutions are

$$(1)\ \Psi < 0 \quad for\ \phi_A < \phi < \phi_B \tag{5.16}$$

$$(2)\ \Psi_A = 0, \quad \Psi_A' = 0, \quad \Psi_B = 0, \quad \text{and} \quad \Psi_B' = 0 \tag{5.17}$$

$$(3)\ \Psi_A'' < 0, \quad \text{and} \quad \Psi_B'' < 0. \tag{5.18}$$

Double layer solutions are guaranteed if the electron and ion distribution functions are such that the resulting Ψ satisfies Eqs.(5.16)–(5.18).

5.3 Particle-in-Cell Simulation of Double Layers

By their very nature, double layers are nonuniform in density and produce particle beams with non-Maxwellian velocity distributions. Moreover, the formation of double layers is a time-dependent problem. For these reasons, the evolution of double layers is often studied by numerical simulation.

Numerical simulation has certain advantages over laboratory experiment and space-satellite observation. Numerical diagnostics do not perturb the system. Additionally, the orbits of the particles and their phase-space densities, easily obtained from simulations, are nearly impossible to obtain from real plasmas, and instantaneous multi-point measurements are impractical in space plasmas and strongly perturbing in the laboratory. Moreover, the electrons and ions can be delineated in a simulation and help to unfold the physical mechanisms at work. This is impossible in real plasmas.

The basic problems of double layers that simulations hope to solve are as follows

(1) What is their geometry and structure and how is this related to the plasma parameters?

(2) What is their generation mechanism?
(3) What are their stability properties?

Double layers have been simulated by two types of computer programs: particle codes and Vlasov codes. In particle codes large numbers of particles are moved according to Eqs.(1.1)-(1.5) (Chapter 8). Vlasov simulations manipulate particle distribution functions $f(\mathbf{x},\mathbf{v})$ which are resolved on a position-velocity grid.

These two methods are equivalent in the limits of infinite numbers of particles, vanishingly small time-steps, and infinite spatial resolution. Each type of simulation has its advantages: boundary conditions on the distribution functions being easier to implement with the Vlasov method and magnetized and multi-dimensional plasmas being easier to analyze with the particle method. We utilize the particle approach throughout; the Vlasov method is reviewed by Borovsky (1984).

5.3.1 Simulations of the Two-Stream Instability

Since current-conducting plasma can form double layers once a threshold in current density is passed, it is of some interest to examine the events leading up to double layers in current flows. The flow of electrons through ions is subject to the Buneman (two-stream) instability as given by the linear treatment of Section 2.7.2. As the formation of a double layer involves trapped populations of electrons and ions, an extension of the linear analysis to quasilinear and nonlinear regimes is necessary.

Some indication that the Buneman instability might lead to double layers is given by the fact that plasma is unstable to an electron-ion two stream instability if the drift velocity of the electrons exceeds the electron thermal velocity, $V_0 > 1.3\ v_{Te}$ [Buneman 1959], while theory [Block 1972, Carlqvist 1972] and experiments [Torvén 1975] have shown the threshold for strong double layers[1] is $V_0 > v_{Te}$.[2] Additionally, both phenomena are electrostatic in nature.

The nonlinear evolution of the Buneman instability was studied by Hirose, Ishihara, and Langdon (1982) who employed a one-dimensional PIC simulation model of a force-free plasma ($E_z = 0$). Under the condition $V_0 >> v_{Te}$ the Buneman instability can develop with the maximum growth rate and frequency,

$$\Gamma = \frac{\sqrt{3}}{2}\left(\frac{m_e}{2m_i}\right)^{1/3}\left[1 - \frac{1}{2}\left(\frac{m_e}{2m_i}\right)^{1/3}\right]\omega_{pe} \tag{5.19}$$

$$\omega = \frac{1}{2}\left(\frac{m_e}{2m_i}\right)^{1/3}\left[1 + \frac{1}{2}\left(\frac{m_e}{2m_i}\right)^{1/3}\right]\omega_{pe} \tag{5.20}$$

at resonance $k\ V_0 = \omega_{pe}$. The Buneman instability is "strong" (i.e., $\Gamma > \omega$). However, the linear regime cannot persist more than a few growth periods because of strong nonlinear effects. These nonlinear effects are (i) the deceleration of the electron beam (anomalous resistivity), (ii) consequent electron heating, (iii) modification of Γ and ω, and (iv) electron trapping.

There are two time scales of interest in the nonlinear evolution of the Buneman instability. The first is the time at which the exponential growth $e^{\Gamma t}$ terminates (Figure 5.7). The second is

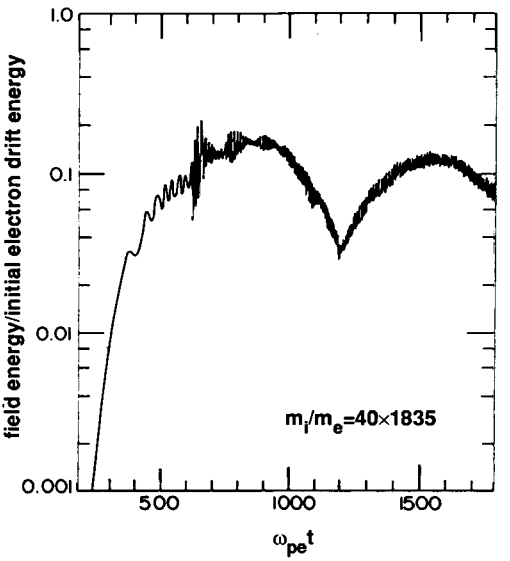

Figure 5.7. Time evolution of electric field energy density for an argon plasma obtained by computer simulation. The system length in the simulation was chosen as one wavelength of the most unstable mode (after Hirose, Ishihara, and Langdon, 1981).

the time when electron trapping sets in. Figure 5.7 shows that after electron trapping begins, the electric field energy density oscillates at twice the ion plasma frequency. (The oscillation has the nature of a standing wave; the electric field and ions exchange energy at this frequency. It is not a complete standing wave since neither field nor ion kinetic energy become zero.) This oscillation is a manifestation of strong ion oscillations at the nonlinear stage of the instability. The role of the Buneman instability is to create large amplitude ion density perturbations at a wavelength that corresponds to the most unstable mode.

The following sequence of events lead to electron trapping. When the field energy reaches a saturation plateau, the electron drift velocity V_0 approaches zero and then takes on negative values. When this occurs, the linear assumption of electrons freely streaming through ions is no longer valid. The electrons begin to reflex in the axial coordinate and rotate in phase space. This is depicted by the phase space vortices as shown in Figure 5.8. The phenomena observed resembles that associated with the Kelvin-Helmholtz fluid instability.

The trapped electrons follow different orbits with different periods due to the nonadiabatic nature of the trapping. This causes the phase space "smearing" seen at later times in the simulation. The region for which $V_0 = 0$ and a substantial number of electrons are reflected backwards is called a *virtual cathode*. Hirose et al. did not observe reflexing in ion motion but did note that the kinetic energy of the ions acquired 10% of the initial electron drift energy.

Boris et al. [1970] studied the two-stream instability when $E_z \neq 0$. In their simulation a current was driven by imposing a axial electric field in the simulation region. They simulated an electron-

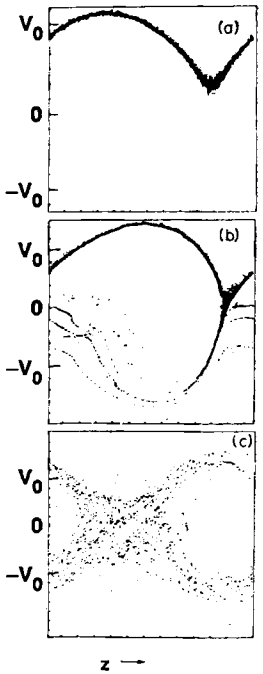

Figure 5.8. Electron phase space diagram. (a) t=38 ω_{pe}^{-1}. (b) t=56 ω_{pe}^{-1}. (c) t=68 ω_{pe}^{-1}.

positron plasma with periodic boundary conditions in both one and two dimensions. The electrons leaving the simulation region to the right, or the positrons leaving to the left, were re-introduced at the opposite boundary at the same exit vertical position (2D) and same exit velocity. Since $m_i = m_e$, the growth rate is large Eq. (5.19) and phase space vortices rapidly appear. Because of the periodic boundary conditions and the axial electric field, collective runaway of some of the electrons was observed. One of their observations was that electron heating by the two-stream instability tended to conserve the condition $v_{Te} \approx V_0$ as the drift velocity increased.

5.3.2 Simulations of Double Layers

Simulations of double layers may involve one or two dimensions in space. The one dimensional system requires far less central processor time but suffers from excluding transverse particle motions associated with expansion or contraction, heat loss at surfaces, and a realistic magnetic field strength (the magnetic field strength may be taken as infinite in a 1D simulation since there can be no transverse losses). Two dimensional simulations may be run with or without the presence of a magnetic field.

To date, almost all PIC simulations of double layers have been electrostatic; again the cost of running a fully electromagnetic simulation is a major consideration.

In PIC simulation, boundary conditions must be specified for both the fields and the particles. For field conditions, one may either specify a particular boundary as being metallic (with tangential electric fields set to zero), wave transmitting as in free-space, or an axis of symmetry. Conductors may be placed at or within the boundaries and their potentials fixed or allowed to float with respect to some reference conductor. The conductors are often made "transparent" to act as grids, so that particles may accelerate through potential gradients. Sometimes a periodic field or potential boundary condition is specified. For this case $\phi(0) = \phi(L)$, where L is the dimension of the system. Since a double layer has a potential drop, periodic field boundary conditions may only be used when the double layer is small compared to the system length.

The particle boundary conditions may be reflecting, absorbing, or periodic. If periodic, $\mathbf{v}_{e,i}(0) = \mathbf{v}_{e,i}(L)$. Much has been learned about the nature of double layers from periodic boundary conditions. However, since the electron and ion beam velocities are unidirectional, the double layer can be simulated only for times shorter than a particle transit time. For this reason, periodic particle boundary conditions do not allow the full growth of double layers.

In nonperiodic simulations neither the potential or the particle velocity vectors are periodic. Nonperiodic simulations can either have a floating or self-adjusting potential, or else have a fixed potential, across the system. The first case corresponds to a constant current source; the second case is a constant voltage source. Both are appropriate to study double layers which appear as elements in an electric circuit.

5.4 Double Layers in Current Filaments

Observations show that electric currents in cosmic plasmas often tend to flow in thin filaments or sheets. Particularly in filaments, the current density may reach comparatively high values. Hence, as suggested by laboratory experiments, the conditions for double layer formation in filaments are optimal.

A double layer that occurs in a current filament cannot, however, be strictly one-dimensional but must constitute a two-dimensional or three-dimensional structure. To clarify the physics of such a layer as studied in 2D simulations, we shall consider the following simple model.

Consider an electric circuit which contains a plasma filament. The filament has the radius of cross section a and carries a current density j_0 so that the total filamentary current is $I_0 = \pi a^2 j_0$. The length scale of the circuit is l implying an inductance of the order $L \approx \mu_0 l$. Hence, the magnetic energy Eq.(3.39)

$$W_B = \frac{1}{2} L I_0^2 \approx \frac{1}{2} \mu_0 l I_0^2 \tag{5.21}$$

is stored in the circuit.

We now assume that a double layer with the potential drop ϕ_{DL} is formed in the filament. Inside the layer, stored magnetic energy is released as kinetic energy of the particles accelerated through the layer. The power developed by the layer is

$$P_{DL} \approx I_0 \phi_{DL} \tag{5.22}$$

Hence, we obtain the time constant for the release of the stored energy

$$\boxed{\tau_B = \frac{W_B}{P_{DL}} \approx \frac{\mu_0 l I_0}{2\phi_{DL}}} \tag{5.23}$$

The ions and electrons accelerated in the double layer form beams when leaving the layer (Figure 5.1). These beams exert a pressure upon the plasma surrounding the layer. As a result of this, the double layer may expand (or explode). The expansion leads to a growing potential drop across the layer and even larger beam pressures.

As long as the double layer has a thickness d that is small compared with its radial extension a, the one-dimensional theory is approximately applicable. However, if the thickness grows larger, a two-dimensional treatment becomes necessary.

In order to get an idea of what the potential drop of the double layer may be in this latter case we consider a capacitor consisting of two circular plates of radius a separated by the distance d. The two plates are charged with the constant surface charge densities $+\sigma_c$ and $-\sigma_c$. When $d << a$ the potential drop between the plates is

$$\phi_C = \sigma_C d / \varepsilon_0 \tag{5.24}$$

(i.e., the same as in a purely one-dimensional geometry). The potential ϕ_C is then proportional to the separation d. For larger separation, ϕ_C grows more slowly with d. Finally, when $d >> a$ the potential drop tends to the constant and maximum value

$$\phi_{C\,m} = \sigma_C a / \varepsilon_0 \tag{5.25}$$

Notice that Eq.(5.25) may be formally obtained from the potential drop in the one-dimensional case by putting $d = a$.

The charge distribution in the relativistic double layer is in several respects similar to the charge distribution in the capacitor considered above. In both cases there is a pronounced charge separation while the total charge is equal to zero. Furthermore, the positive "surface" charge density at the anode boundary of the relativistic double layer appears to be independent of the thickness of the layer, just as the surface charge density of the capacitor is independent of the separation between the plates. Hence, when the thickness of the double layer d is much larger than the radius a we should expect the potential drop of the layer to approach the maximum value

$$\phi_{DL\,m} = \left(\frac{\phi_i j_0 a^2}{4 \varepsilon_0 c} \right)^{1/2} \tag{5.26}$$

corresponding to the one-dimensional potential drop given by Eq.(5.12) with $d = a$ and $j = j_0$. In terms of the filamentary current I_0, Eq.(5.26) may be rewritten as

$$\boxed{\phi_{DLm} = \left(\frac{\phi_i I_0}{4\pi\varepsilon_0 c}\right)^{1/2}} \tag{5.27}$$

Thus, the maximum potential drop of the relativistic double layer is a function of the *total current* rather than of the current density. In Figure 5.4 ϕ_{DLm} is shown as a function of I_0 in the relativistic regime.

The potential ϕ_{DLm} as described by Eq.(5.27) constitutes the maximum potential drop that can be *sustained* by the double layer. One condition for ϕ_{DLm} to be approached is, as we have seen above, that the double layer expands so that its thickness becomes larger than its radius. There is, however, another condition which depends on the *circuit* that also has to be fulfilled if ϕ_{DL} is to approach ϕ_{DLm}. Due to the fact that the magnetic energy stored in the current filament cannot be released faster than the Alfvén travel time Eq.(2.22) along the filament, there is an upper limit to the power that can be supplied by the circuit. For ϕ_{DLm} to be reached, this power has to be at least equal to the maximum power of the double layer $I_0\phi_{DLm}$. This condition seems to be well met in cosmic circuits.

5.5 Basic Properties of Double Layers

5.5.1 Double Layers as a Surface Phenomena

If an electrical discharge is produced between an anode and a cathode (Figure 5.9), a cathode sheath forms near the cathode and serves to accelerate electrons that carry a current through the plasma. This sheath, a "virtual cathode," is one layer of the double layer. Similarly, a "virtual anode" is set up near the anode, protecting the plasma from this electrode. Again, a space charge layer constitutes the border between the double layer and the plasma. The double layers carry electric currents.

The lateral limitation of the plasma is also produced by double layers, which reduce and slow the escape of fast electrons and also accelerate ions outwards, so that ambipolar diffusion is established (no net current). The walls of an enclosing vessel take on a negative charge while a positive space charge layer forms to act as a border between the double layer and the contained plasma. If the discharge constricts itself, the walls can be removed (without removing the space charge), and the net electric current is zero in the lateral double layers.

If the plasma is inhomogenous in chemical composition, density, and electron temperature, double layers may form to "cellularize" the plasma into regions which are, more or less, homogeneous. For example, Birkeland currents flowing between the ionosphere and magnetosphere may produce a series of double layers as the currents flow through regions with different densities.

There are innumerable variations and complications of the cases we have discussed, just as biological cell walls show innumerable variations. Another example of this is the formation of a double layer when the current through a plasma is increased by increasing the applied voltage. The double layer so formed takes up part of the voltage and thereby "clamps" the current to some

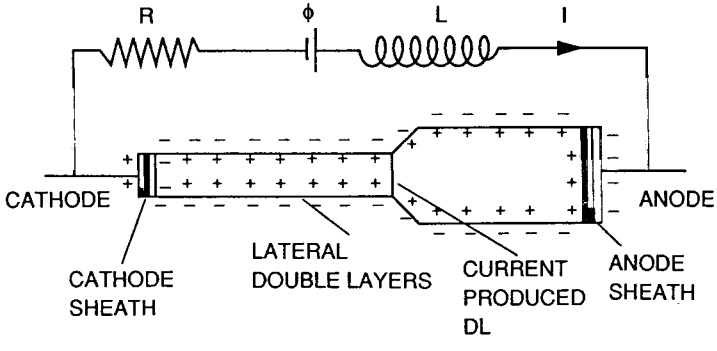

Figure 5.9. Sheathes and double layers associated with an electric discharge.

threshold value. Hence, the plasma divides itself into two cells, analogous to what a biological cell does when it gets a large energy input.

The voltage difference $\Delta\phi$ over a double layer is usually of the order 5–10 times the equivalent of the temperature kT_e/e. However, if there are two independent plasmas produced by two different sources, the energy may be as high as 100-1,000 kT_e/e in the double layer produced between the plasmas.

5.5.2 Noise and Fluctuations in Double Layers

Concomitant with double layers are noise and rapid fluctuations. Lindberg [1982] found that noise (i.e., rapid variations within a broad spectral band) was associated with a broadening of the energy spectrum of the electrons. The effect of noise is to scatter the electrons in the beam that is produced within a double layer so that plasma expansion across the confining magnetic field is possible. The noise scattering mechanism can greatly exceed the scattering due to collisions between electrons.

5.5.3 Exploding Double Layers

Since double layers form in electrical currents, the double layer itself can be considered an element within the complete electrical circuit. Figure 5.10a depicts a simple series circuit in which a current I flows that contains a generator, motor, resistance, inductance, and a double layer.

If $\phi > 0$, we have a generator transferring plasma power ϕI into the circuit; if $\phi < 0$ we have a motor transferring circuit energy into kinetic energy of the plasma. The circuit also has a resistance R which dissipates power I^2R into heat, and an inductance L in which circuit energy is stored [Eq.(3.39)].

In most cosmic plasma situations the individual circuit elements must be replaced with elements that are distributed over cosmic distances. Thus, even the conducting "wire" itself, connecting the circuit elements, must be replaced by a transmission line representation of the current-carrying, field-aligned, pinched cosmic plasma filament conductors (Appendix A).

Every circuit that contains an inductance L is intrinsically explosive. The inductive energy Eq.(3.39) can be tapped at any point of the circuit. Any interruption of the current I results in the

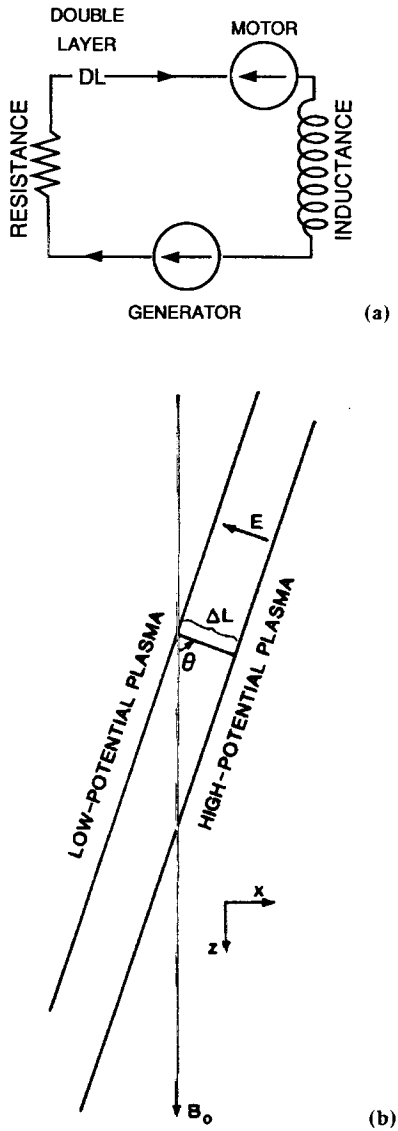

Figure 5.10. (a) Series circuit containing a voltage source, resistance, inductance, motor, and double layer. Circuit energy in the "motor" is used to accelerate the plasma. (b) The coordinate system of an oblique double layer. The angle between the double layer normal and $\mathbf{B}_0$ is denoted as $\theta = \theta_{DL}$.

transfer of the inductively stored energy to the point of interruption. By its nature, this point is most often a double layer which then releases energy at a rate

$$P = I\ \phi_{DL} \tag{5.28}$$

where ϕ_{DL} is the voltage drop across the double layer. This energy is mainly used for accelerating charged particles, with a small percent released in the generation of noise. Secondary effects associated with the particle acceleration include localized heating and radiation.

5.5.4 Oblique Double Layers

In space, double layers are often associated with magnetic fields, and the trajectories of the double layer electrons and ions are influenced by **B**. When the double layer field **E** is not parallel to **B**, the magnetized double layer is referred to as an *oblique* double layer (Figure 5.10b) [Borovosky 1984].

Magnetized double layers usually have scale thicknesses of approximately $20\lambda_D$ (where λ_D is the Debye length of the hottest species of particles passing through the DL), regardless of their orientation with respect to **B** (an exception occurs if **E** is not precisely perpendicular to **B**). Depending on the properties of the plasma on either side of the DL, the oblique magnetized DL will drift at velocities up to the ion acoustic speed. Owing to the transfer of momentum from the beam to the electrons in the high-potential plasma via two-stream instabilities, the predominant direction of the DL drift is in the direction of the emitted electron beam. The orientation of fields in Figure 5.10b, when applied to a sheet beam geometry, makes the oblique DL a naturally ocuring analog of the smooth bore magnetron (Section 1.7.3).

5.6 Examples of Cosmic Double Layers

5.6.1. Double Layers in the Auroral Circuit

The auroral circuit is by far the best known of all cosmic circuits. It is derived from a large number of measurements in the magnetosphere and in the ionosphere. A simplified schematic of the picture that has evolved of the auroral circuit is shown in Figure 5.11. Magnetospheric convection produces an emf ϕ_0 which drives a field aligned current $j_\parallel$. The ionosphere is represented by a resistance R. DLs form in the plasma region to produce a field-aligned electric field which accelerates electrons and ions in opposite directions.

On auroral field lines, the current-carrying electrons and the oppositely streaming ions are governed by conditions external to the double layer and therefore can be specified fully as boundary conditions for simulations. The trapped ions on auroral field lines are mostly plasma-sheet thermal ions of keV energy on the low-potential side of the double layer; therefore the distribution function of the trapped ions can be specified externally as a boundary condition. On the other hand, the trapped electrons on auroral field lines with sufficient energy to penetrate deep into the double layer are produced mostly by the backscattering of the streaming electrons due to charge-neutral collisions in the ionosphere on the downstream side of the double layer; or are a combination of both. The ionospheric electrons of energy less than 1 eV are of no consequence because they are

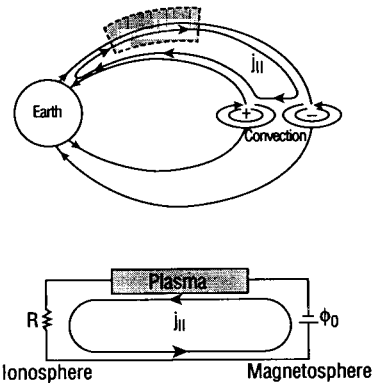

Figure 5.11. (top) A model of coupled magnetosphere-ionosphere system. **(bottom)** Equivalent circuit representation (adapted from Sato and Okuda 1981).

unable to contribute to the space charge inside the double layer. Therefore, the trapped electrons can not be prescribed as a boundary condition.

Since the trapped ions and the streaming electrons and ions on auroral field lines can be specified as boundary conditions, one can determine the density of the trapped electrons as a function of ϕ from Eqs.(5.16)–(5.18) for ψ for the existence of double layer solutions. This result provides an explicit constraint on the distribution function of the trapped electrons, but still cannot answer the question on realizability of the solution. To answer this question unambiguously, one must treat the double layer formation as an initial value problem so that the production of the trapped electrons can be followed in time. The transition from a localized DL to an extended DL has been shown to depend predominantly on the energy of the trapped electrons [Kan and Akasofu 1989].

An immediate question that comes to mind is what controls the field-aligned scale length of a double layer. The boundary conditions on the ionospheric side of the auroral double layer are uniquely different from the classic double layer. First, the converging geomagnetic field is favorable for retaining the trapped particles on the ionospheric side. Secondly, the partially ionized ionosphere is a source of trapped particles due to the backscattered primary and secondary electrons produced by the auroral electrons. This is in contrast to the classic double layer in which the trapped particles can only be produced by instabilities, and with no magnetic mirror to help maintain the trapped-particle population.

Figure 5.12 shows the double layer simulations results of Yamomoto and Kan (1985). The field-aligned scale length $L_{\parallel}$ of a double layer varies from (a) localized to about a ten Debye lengths in the absence the backscattered primary electrons and the hot magnetospheric ions, to (b) a partially extended in the presence of the backscattered primary electrons, and (c) to become fully extended across the entire simulation domain if both the backscattered primary electrons and the magnetospheric hot ions are present. Figure 5.12d shows that the fully extended double layer remains fully extended under the same condition as in Figure 5.12c except that the length of the simulation domain is double in length. This result clearly indicates that the field aligned scale

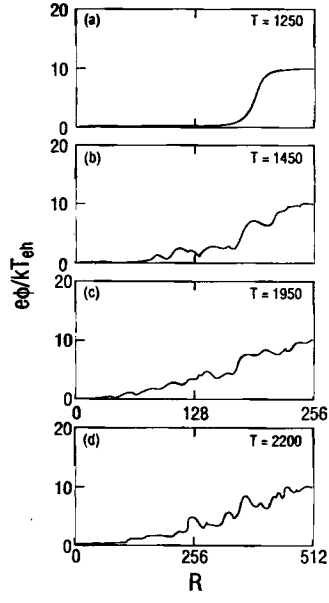

Figure 5.12. Simulation results on the variation of the field-aligned scale length of a double layer. The right hand potential is fixed at 10.0.

length of a double layer is controlled by the energy of the trapped-particle populations. The scale length increases as the energy of the trapped-particle population increases.

Oblique DLs (Section 5.5.4) have been suggested as causes of ion conics (beams of ions whose angular distributions have a minima in the field-aligned direction), and auroral kilometric radiation [Borovosky 1984, 1988].[3] Figure 5.13a illustrates the trajectories of various magnetized initially magnetic field-aligned ions passing through an oblique DL. In unmagnetized DLs, the ion motion is along **E**. As the strength of the magnetic field increases, the ion trajectories become increasingly aligned along **B**. In studying ion conics, Borovosky finds a transition between electric field alignment and magnetic field alignment in the parameter range $2.18 \leq \omega_{ci}\, \tau_{cr} \leq 8.72$, where τ_{cr} is the time required for an ion to be accelerated across the oblique DL.

Simulations of oblique DLs show electromagnetic wave properties similar to that of AKR [Borovosky 1988]. The emitted waves have frequencies slightly above and slightly below the local electron cyclotron frequency (f_{ce}~30 kHz, λ_{ce}~10 km), and the waves are emitted primarily in the north-south (constant longitude) direction. In the auroral zone, the DL drift in the electron sheet beam direction, carries it along the terrestrial magnetic field, toward the poles (Figure 5.13b). Borovosky (1988) finds a power of P~1.2×10^6 W per discrete auroral arc element. The observation that a typical arc consists of 5 elements requires the presence of 16–160 arcs in the auroral zone to produce 100 MW–1 GW of AKR. The total efficiency of auroral arc electron kinetic energy

into electromagnetic radiation is ~0.5% (smooth bore magnetrons typically achieve efficiencies of a few percent).

5.6.2 Solar Flares

Solar flares are the result of a sudden irreversible release of energy in the corona and chromosphere of the sun. These lead to particle acceleration observed mainly in the range 10^4–10^5 eV, and to a transient heating of the chromosphere [to $\approx$ 1 eV (10^4 K)] and corona [to $\approx$ 10^3 eV (10^7 K)]. Electromagnetic radiation is produced over an extremely broad range from radio up to X and even γ ray frequencies.

A typical flare passes through a sequence of phases. There is an initial preflare or preheating phase lasting around 10 min characterized by a slow optical brightening with an accompanying rise in the extreme ultraviolet (EUV) and soft X ray emission. This is followed by a short explosive or impulsive phase ($\approx$1 min) during which there are impulsive emissions of hard X rays, EUV, and microwaves (i.e., the most energetic nonthermal events). There is a rise to maximum brightness and emission in soft X rays and EUV during the 5–15 min flash phase, followed by a slow decline in the main phase (~1 hour). Flashes occur mainly in active regions, containing sunspots and a generally enhanced magnetic field, and are believed to derive their energy through this field. There are strong arguments for the storage of energy in the magnetic field [i.e., as inductive energy in an extended current system (Section 3.7)].

Estimates of the energy release due to changes in the magnetic field topology are of the right order of magnitude. The total energy released in a flare is in a range extending over more than three orders of magnitude, from $\approx 10^{22}$ J for a typical subflare to $\approx 3 \times 10^{25}$ J in the most energetic cases. For large flares this energy is roughly equally divided between electromagnetic radiation, energetic particles, and shock waves propagating outward into the solar wind region [Priest 1982]. Flare "areas" are reported for the extent of the H_α emission at maximum intensity and range from less than 3×10^8 km^2 for subflares, and from 7.5×10^8 km^2 to over 3.6×10^9 km^2 for major flares. High-resolution observations reveal small (diameter ~ 3,000–6,000 km) impulsive flare kernels with enhanced brightness associated with the X ray bursts. Small-scale "compact" flares may take the form of simple loops accompanied in some cases by surges. The much larger "two-ribbon" flares, so called from the pair of H_α emission regions in the form of long ribbons observed during the flash phase, are closely associated with a prior filament destabilization and eruption.

Currents in the solar atmosphere are inferred from magnetic field measurements. If the magnetic field $\mathbf{B}$ is known, the current density $\mathbf{j}$ can be derived from Eq.(1.2), $\nabla \times \mathbf{B} = \mu_0 \mathbf{j}$. By measuring the transverse component of the magnetic field Severney (1965) found that vertical currents of the order of 10^{11} A exist in the neighborhood of sunspots.

Moreton and Severny (1968) have pointed out a remarkable coincidence between the bright knots appearing during the initial phase of flares and spots with a vertical current density larger than 8×10^{-3} A m^{-2}. The currents can either flow outward or inward from the spots. The measured diameter of the spots is comparable with the observational resolution ~7" corresponding to a distance ~5×10^6 m on the sun. With a current density $j = 8 \times 10^{-3}$ A m^{-2} and with a diameter of the current elements of 5×10^6 m one obtains a total current of $I \sim 2 \times 10^{11}$ A.

Since the apparent diameters of the spots are of the same order as the resolution it is possible that the real diameter might be still smaller. This would lead to an enhanced current density compared with the measured one.

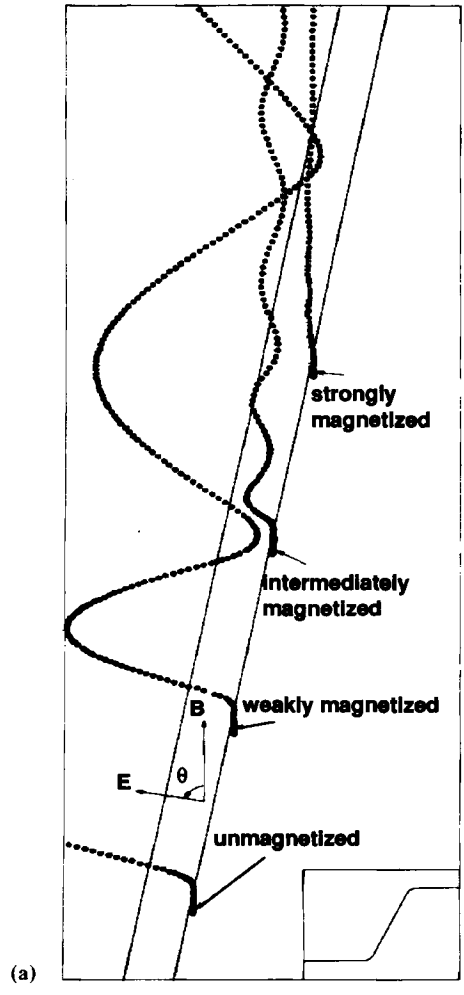

Figure 5.13. (**a**) The trajectories of variously magnetized initially field-aligned ions passing from the high-potential plasma through an oblique (θ_{DL} = 79.7°) double layer. The functional form of the double layer is contained in the inset to the bottom right. (**b**) Schematic (not to scale) of an auroral double layer and some of the phenomena it produces. An actual auroral double layer is only a few kilometers in north-south (constant longitude) extent, and may be one in a chain of many double layers. (**c**) Model of a solar flare. The lower boundary is the high-density photosphere. The energy stored in a twisted magnetic flux loop in the corona is released by a double layer.

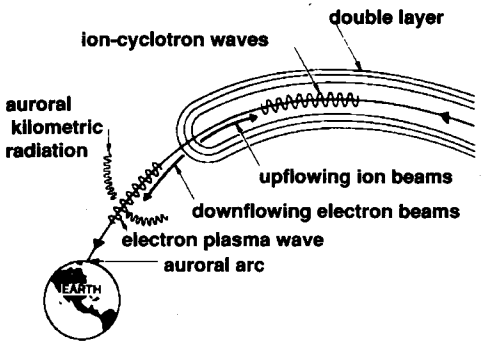

(b)

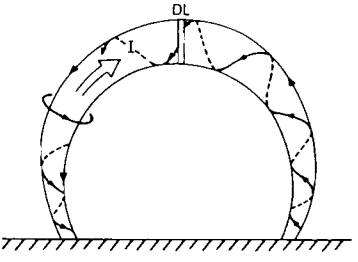

(c)

In the corona and in most of the chromosphere the magnetic pressure $p_B = B^2/2\mu_0$ far exceeds the kinetic pressure of the plasma as soon as the magnetic field is larger than $\approx 10^{-3}$ T (10 G). This implies that any stationary current system inducing magnetic fields larger than $\approx 10^{-3}$ T, must be nearly force-free with the current almost parallel to the magnetic field. Otherwise kinetic pressure forces cannot balance the $\mathbf{j} \times \mathbf{B}$ forces. For example, a current of the order of 2×10^{11} A, constricted to an area with a diameter equal to or less than 5×10^6 m, must be force-free since it induces a magnetic field larger than 10^{-2} T (10^2 G).

As shown in Section 1.7.2, a force-free current system has a tendency to form a narrow filament with most of the total current and magnetic flux confined within it. Inside the filament the magnetic-field lines will assume helical shapes.

The results obtained by Moreton and Severny (1968) indicate that such a current filament can pass from one point in a sunspot group through the chromosphere and through the lower corona and then back again to another point in the same group (Figure 5.13c). Hence, the length of the filament l should be comparable with the typical dimension of a sunspot group $\sim 10^7$–10^8 m. The current circuit might finally be closed in the deeper layers of the solar body where non-force-free conditions prevail.

Example 5.1 Electrical properties of solar flares. The magnetic energy stored in a current system is given by Eq.(3.36). It is convenient to use the inductance $L = L_{int} + L_{ext}$ and derive the energy from

$$W_B = \frac{1}{2} L I^2 = \frac{1}{2} L_{int} I^2 + \frac{1}{2} L_{ext} I^2$$

where the first and second terms correspond to the magnetic energy stored inside and outside the filament, respectively.

For a circular current loop of radius R consisting of a current channel of radius a, the internal and external inductances in vacuum are

$$L_{int} = \frac{11}{24}\mu_0 R$$

and

$$L_{ext} = \mu_0 R\,[ln\ 8R/a - 2]\,; \quad R >> a$$

The distribution of the current density is assumed to be $j \propto (a^2 - r^2)$ for $r \leq a$ resembling that of the force-free filament.

We can now use the circular loop as a model of the current filament in the solar atmosphere in order to estimate the inductance of the filament. Because of the high conductivity of the solar atmosphere it is likely that a considerable part of the magnetic field outside the filament will be screened by the plasma. The external inductance of the filament may therefore be much reduced compared with the vacuum case. On the other hand, the internal inductance of the current filament would be comparable with the internal inductance of the circular current loop. With a radius of the current filament $\approx l/2 \approx 5 \times 10^6 - 5 \times 10^7$ m, we then obtain an inductance of the filament of the order of $L \approx 3$–30 H.

The total filamentary current needed to produce a stored magnetic energy comparable with the energy of a flare $W_f = LI^2/2 \approx 10^{21}$-$10^{25}$ J is in the range $I \approx 10^{10}$-10^{12} A.

If we assume that the filamentary current is mainly carried by electrons and protons, the maximum potential drop of a double layer in the filament is, according to Eq.(5.27), $\phi_{DLm} \approx 9 \times 10^{10}$ V (90 GV). The time constant for energy release connected with this potential drop is from Eq.(5.23) $\tau_B \approx 2 \times 10^2$ s.

It is to be noticed that both W_B and τ_B in Example 5.1 are of the same magnitudes as the total energy and the time constant of solar flares, respectively. Hence, the double layer constitutes a mechanism that is capable of releasing the flare energy during the brief explosive phase observed.

The analysis of observations from the Solar Maximum Years have led to an improved understanding of the build-up phase of solar flares and of the energy release. Hard X ray and microwave bursts have been found to have fine structure on time scales of a few tens of milliseconds. During the impulsive phase, hard X ray emission is observed at the foot of loops with microwave emission from the tops. Of particular interest for models with acceleration by strongly relativistic DLs is the observation of energetic neutrons (50–500 MeV, where the upper limit is uncertain and may be much greater) produced during the impulsive phase. The DL model is able to meet the rather stringent requirements for the acceleration mechanism set by the observations, both as regards to the time scale and number of high-energy protons which produce the neutrons [Carlqvist 1986]. Further evidence of acceleration to very high energies comes from observations of γ ray emission due to protons [Ryan et al. 1983]. In the context of these results the DL has the advantage of accounting for the acceleration to very high energies and allowing extremely rapid time variations, since its structure can vary on the local ion transit time scale.

5.6.3 Double Radio Galaxies and Quasars

Double layers produce beams of electrons and, on astrophysical scales, these beams are relativistic. The beams are also directed along $\mathbf{B}_0$ so that the expected loss mechanism for the beam kinetic

energy is synchrotron radiation. The formation of a series of DLs in a network of current-conducting plasmas thus leads to an interesting problem regarding total synchrotron intensity, background radiation levels, and isophotal patterns. This problem is addressed in some detail in Chapter 6.

5.6.4 Double Layers as a Source of Cosmic Radiation

It is of interest to compare the cosmic particle acceleration discussed in Section 5.6.2 with some energetic cosmic particle observations. Very energetic particles—primarily protons—are recorded on earth following large solar flares. The proton energies can be many tens of GeV after such an event.

It has been demonstrated by Chupp et al. (1982) that the sun also emits neutrons of high energy. Just after a solar γ ray impulsive burst, indicating the onset of a strong ($1B$) flare, neutrons with energies at least as high as 6×10^8 eV were detected at the earth. The production of such neutrons requires that protons be accelerated to GeV energies, probably within a 20 s time interval corresponding to the impulsive phase. As pointed out by Chupp et al., this short time imposes a strong constraint on the properties of the particle accelerator operating in the flare region.

In Section 5.6.2 we found that a double layer in a solar filament carrying the current $I = 3 \times 10^{11}$ A can sustain a maximum potential drop of about $\phi_{DLm} \approx 9 \times 10^{10}$ V. This means that such a layer is capable of accelerating particles to energies that correspond to the highest solar cosmic ray energies observed.

As regards the high-energy neutron event detected by Chupp et al., a solar double layer seems to meet the very special requirements on the acceleration mechanism imposed by the observations. First, the double layer is able to accelerate a fairly large flux of protons, $\psi_p \approx 10^{30}\,\mathrm{s}^{-1}$. Second, the time of acceleration of each particle in the layer is very short—only a fraction of a second. Hence, the total number of protons $N_{20} = 20\,\psi_p = 2 \times 10^{31}$ of GeV energy can be directly produced by the double layer during the 20 s time interval of the impulsive burst. In addition to this, it is likely that many more particles of lower energy are generated by the primary particles through secondary processes in the solar atmosphere.

Example 5.2 Electrical properties of galactic pinches. Consider a double layer in a galactic filament conducting 10^{20} A (Example 6.7). For a proton-electron plasma, Figure 5.4 gives a value $\phi_{DL} \approx 3 \times 10^{17}$ V in the relativistic regime. If the voltage is actually distributed over a series of double layers extending for 10 kpc in the filament, the average electric field strength is 1 mV/m. The total energy of an ion that has been accelerated through the double layers is 3×10^{17} eV. This energy is similar to that derived by Vlasov, Zhdanov, and Trubnikov (1989) for pinched plasma currents as a source of cosmic rays. The time constant for the release of energy Eq.(5.22) is $\tau_B = 2 \times 10^9$ years. The time rate of energy release Eq.(5.28) is 3×10^{37} W.

Notes

[1] A DL is said to be "strong" if the energies acquired by the ions and electrons accelerated by the potential difference ϕ_{DL} are very large compared to the energies of the incoming and reflected particles. The internal DL structure is then determined by the accelerated particles, which may be treated approximately as cold beams.

[2] This *Bohm Criterion* is a condition for existence of strong double layers with a Maxwellian distribution of trapped ions.

[3] Auroral kilometric radiation (AKR) (Section 1.8.1) is bursty electromagnetic emission originating in the dusk and evening auroral zone at geocentric radii of 2 to 4 R_e. The radiation is believed to be emitted at frequencies near the local electron cyclotron frequency. The power levels of AKR emission are highest during times of geomagnetic activity, and the emission is correlated with the presence of precipitating high-energy electrons, with the presence of Birkeland currents, and with the presence of auroral arcs. The radiation is believed to be emitted with wave vectors that are nearly perpendicular to the terrestrial magnetic field, but tilted slightly earthward. It is also thought that the extraordinary mode dominates in AKR. Because of the rising or falling in frequency of the bursts, the source region is envisioned to move down or up the terrestrial magnetic field at approximately the local ion acoustic speed.